Solid State Ionics 31 (1988) 31–40
North-Holland, Amsterdam

SODIUM AND OXYGEN DISORDER IN A SCANDIUM-SUBSTITUTED NASICON: A TIME OF FLIGHT NEUTRON POWDER DIFFRACTION STUDY OF $Na_{2.5}Zr_{1.8}Sc_{0.2}Si_{1.3}P_{1.7}O_{12}$

Philip J. SQUATTRITO, Philip R. RUDOLF, Paul G. HINSON, Abraham CLEARFIELD *
Department of Chemistry, Texas A&M University, College Station, Texas 77843, USA

and

Kenneth VOLIN and James D. JORGENSEN
Materials Science and Technology Division, Argonne National Laboratory, Argonne, Illinois 60434, USA

Received 23 May 1988; accepted for publication 26 June 1988

A Sc-substituted NASICON of composition $Na_{2.5}Zr_{1.8}Sc_{0.2}Si_{1.3}P_{1.7}O_{12}$ has been prepared and characterized by neutron powder diffraction and conductivity measurements. Time-of-flight neutron powder diffraction data were collected at 26, 100, 200, 300, and 400°C. Satisfactory Rietveld refinements were obtained for all temperatures using the rhombohedral space group $R\bar{3}c$. The novel aspect of this structure is the simultaneous presence of partially occupied interstitial sodium and oxygen sites that are disordered with the regular Na(2) and O(1) sites in the known rhombohedral NASICON structure. The results are compared with recent findings of defect structures in other NASICON materials. Conductivity measurements in the range 30–350°C reveal an activation energy of 0.30 eV for Na^+ conduction but conductivity values were found to change with temperature of sample preparation.

1. Introduction

NASICON [1,2] is the generic name of a family of zirconium silico-phosphates containing highly mobile sodium ions. The structure consists of a three-dimensional framework of ZrO_6 octahedra and $P(Si)O_4$ tetrahedra with the sodium ions occupying intervening cavities. The distribution of the sodium ions in these sites and their ability to hop from one cavity to another is the basis for the ionic conductivity. The original description of NASICON was as a solid solution of composition $Na_{1+x}Zr_2Si_xP_{3-x}O_{12}$ [1,2]. The end members, $x=0$ and $x=3$, crystallize in the rhombohedral space group $R\bar{3}c$ and exhibit low Na^+ conduction. However, the conductivity increases with x to a maximum at $x\simeq 2$. In the range of highest conductivities, $1.6<x<2.3$, the structure distorts to monoclinic, space group C2/c. This variation of conductivity with composition is believed to be the result of two competing effects. Firstly, widening of the passageways between the cavities as the larger Si^{4+} replaces P^{5+} causes an enhancement of the conductivity [3,4]. Secondly, as the occupancy of the Na^+ sites increases, the conductivity first increases and then falls off as the cavities become filled.

In earlier structural studies [5–7] it was shown that Na^+–Na^+ repulsions play an important role in how the cavities fill, thereby affecting the resultant conductivity. Other studies [5–11] have indicated that deviations from the stoichiometry originally proposed [2], involving substitution of Na^+ for some of the Zr is possible. This Zr replacement leads to a new general formula, $Na_{1+x+4y}Zr_{2-y}Si_xP_{3-x}O_{12}$ [5,9]. The nonstoichiometric phases appear to display the same structural correlations with conductivity as the stoichiometric ones. Other less dramatic deviations from the strict stoichiometry required by Hong's formula have also been observed [6,7,12].

* Author to whom correspondence should be addressed.

0 167-2738/88/$ 03.50

All of these deviations have been attributed to the fact that equilibrium was not attained during sample preparation and that the end product depended upon the preparative method [6,13,14]. It has now been shown that long annealing of some of these nonstoichiometric phases leads to the formation of crystals which strictly adhere to Hong's formula [15,16]. However, these annealed crystals contain some of the Na^+ in a new interstitial site.

Prior to these latter publications [15,16], we undertook a comprehensive structural study of NASICON phases in which Zr^{4+} is partially replaced by Sc^{3+} [17]. This substitution allows the P/Si ratio to vary independently of the Na^+ concentration but as there is no concomitant substitution of Na^+ in the Zr/Sc site (*vide infra*) the Sc-substituted NASICONS are stoichiometric. We report here the results of a multi-temperature neutron time-of-flight study of a phase with composition $Na_{2.5}Zr_{1.8}Sc_{0.2}Si_{1.3}P_{1.7}O_{12}$. The results are compared with those of the recent single crystal work [15,16] and with other findings of interstitial sodium and oxygen positions [11,18].

2. Experimental

2.1. Synthesis and characterization

Starting materials used: ZrO_2 (Aldrich, 99.99%); SiO_2 (Alfa, 99.99%); Sc_2O_3 (Aldrich, 99.999%); ZrP_2O_7 (prepared from α-zirconium phosphate, $Zr(HPO_4)_2 \cdot H_2O$, as described previously [19]); $Na_3PO_4 \cdot 12H_2O$ (Fisher, 99.9%). All chemicals were dried for 48 h at 200°C prior to use. Stoichiometric quantities of starting materials were ground together in a synthetic sapphire mortar until thoroughly mixed. The resulting mixture was transferred to a platinum crucible and heated for ~30 min at 200°C. The temperature was slowly raised to 1050°C and maintained for 12 h. This procedure was followed by two more cycles of grinding and heating to try to ensure a homogeneous sample. An X-ray powder diffraction pattern recorded on a Seifert-Scintag PAD-II computer-automated powder diffractometer (CuKα, $\lambda = 1.5418$ Å) revealed the presence of a small amount (~2 wt%) of unreacted ZrO_2. X-ray fluorescence analysis (Philips Electronics) of the sample gave 10.87% Na, 32.52% Zr, 1.34% Sc, 7.38% P and 5.69% Si. Calculated for $Na_{2.5}Zr_{1.8}Sc_{0.2}Si_{1.3}P_{1.7}O_{12}$: 11.23% Na, 32.09% Zr, 1.75% Sc, 10.28% P and 7.14% Si. It is evident that the analysis for P and Si is low, but their ratio 1.62:1.38 is close to that required by the formula. Only by increasing the observed values for P and Si by 30% does the sum of the oxides equal 100%.

2.2. Conductivity measurements

Ionic conductivity measurements and data analysis were performed on the $Na_{2.5}Zr_{1.8}Sc_{0.2}Si_{1.3}P_{1.7}O_{12}$ sample following previously described procedures [17].

2.3. Crystallographic study

Time-of-flight, TOF, neutron powder diffraction data were collected on the Special Environment Powder Diffractometer (SEPD) [20,21] at the Intense Pulsed Neutron Source (IPNS) of Argonne National Laboratory. The sample was loaded into a cylindrical vanadium sample holder (vol. ~5.2 cm^3) under an inert dry atmosphere. The holder was sealed by an indium gasket. Cadmium shielding was used to eliminate scattering from the aluminum end caps of the can and the support fixture. Data were collected at 26, 100, 200, 300, and 400°C (estimated error ±1°C) using a temperature programmed furnace. Up to 2 h equilibration time was allowed at each new temperature in case a phase change occurred. The data obtained from the back scattering (151°) detector banks were used in the refinements. The starting model used in each of the refinements was the room temperature rhombohedral structure of $Na_3ZrScSiP_2O_{12}$ [17] for the major phase and the monoclinic (room temperature, single crystal) structure of ZrO_2 [22] for the minor phase. The 2.5 Na atoms were statistically distributed over the two crystallographically independent available sites. Rietveld refinements were performed on a VAX 11/780 computer using the IPNS Rietveld analysis programs [23]. The latest version of the least-squares analysis program allows for the simultaneous refinement of up to 4 phases and includes a modified 6-term background function. Similar procedures were followed for all the refinements. The data range used

was 6200–26000 μs (0.82–3.44 Å). In each case the cell parameters, scale, and peak shape of the ZrO_2 were refined together with the structural parameters of the NASICON phase.

Difference Fourier maps calculated after the starting positional and thermal parameters had been refined to convergence revealed the presence of sizable residual peaks near O(1) and Na(2). The first was added to the refinement as O(1′) and its population was tied to that of O(1). After convergence, the second peak was added as Na(2′) with its occupancy constrained with that of Na(2). This refinement converged smoothly and subsequently the anisotropic thermal parameters of the Na ions were refined. During the latter stages of the refinements, the positional parameters of the ZrO_2 were refined with those of the NASICON fixed. Final refinements for each temperature for the NASICON phase included positional parameters for all atoms, isotropic thermal parameters for all non-sodium atoms, and population parameters for Na(1), Na(2)/Na(2′), and O(1)/O(1′). Attempts to refine the population of the Zr/Sc site indicated no significant deviation from the assumed stoichiometry.

3. Results

3.1. Structural results

Final refinement parameters for all the data sets are given in table 1. Positional, thermal, and occupancy parameters are listed for the five temperatures in tables 2–6. Selected metrical data appear in table 7. Final Rietveld profile plots for two of the temperatures are shown in figs. 1 and 2. The most significant result of this study is the observation of positional disorder for Na(2) and O(1) of the rhombohedral NASICON structure. The interstitial sodium position, Na(2′), is displaced ca. 1 Å from Na(2) toward Na(1) as shown in fig. 3. Taking account of the site multiplicities, the refined populations indicate an approximate 50/50 split between the two sites that is independent of temperature. Despite their spatial proximity, the two sodium sites have quite different coordination environments. Atom Na(2) is 8-coordinate with regular Na–O bond distances. By contrast Na(2′) is in 6-fold coordination consisting of 4 O(2) atoms and two O(1)/O(1′) atoms. Moreover, there is an apparent interaction between Na(2′) and O(1) of ca. 2.1 Å, significantly shorter than the 2.40 Å predicted for 6-coordinate sodium from ionic radii [24]. However, the refined populations of Na(2′) and O(1) (tables 2–6) are such that their sum is less than 100% at all temperatures studied, so the disorder between O(1) and O(1′) may preclude the presence of such an unfavorable interaction in the structure. As shown in table 7, if this interaction is neglected, the Na(2′)–O distances appear far more regular. The interstitial oxygen atom O(1′) is located ca. 0.5 Å from O(1). Unlike those of atom Na(2′), the positional and population parameters of O(1′) show apparent correlations with temperature. As the temperature is increased, O(1′) moves away from O(1) (table 7) while at the same time, the occupancy of O(1′) di-

Table 1
Refinement parameters for each temperature.

Temperature (°C)	Space group	a(Å)	c(Å)	V(Å^3)	No. of contribut. reflections (NASICON/ZrO_2)	R_p[a]	R_{wp}[b]	R_e[c]
26	R$\bar{3}$c	8.9834(1)	22.8658(5)	1589.09(3)	650/289	0.0373	0.0504	0.0272
100	R$\bar{3}$c	8.9844(1)	22.9145(4)	1601.83(3)	651/287	0.0323	0.0438	0.0257
200	R$\bar{3}$c	8.9852(1)	22.9698(4)	1606.00(3)	651/287	0.0308	0.0420	0.0251
300	R$\bar{3}$c	8.9863(1)	23.0161(4)	1609.62(2)	652/288	0.0296	0.0412	0.0239
400	R$\bar{3}$c	8.9876(1)	23.0560(3)	1612.87(2)	658/288	0.0282	0.0389	0.0201

[a] $R_p = \sum_i [Y_i(\text{obs}) - Y_i(\text{calc})] / \sum_i [Y(\text{obs}) - \text{bkg}_i]$.
[b] $R_{wp} = \{\sum_i w_i [Y_i(\text{obs}) - Y_i(\text{calc})]^2 / \sum_i w_i [Y_i(\text{obs})]^2\}^{1/2}$.
[c] $R_e = \sqrt{\text{df} / \sum_i W_i [Y_i(\text{obs})]^2}$.

Table 2
Positional, thermal and population parameters for 26°C refinement.

Atom	x	y	z	Biso/Beq	Pop.
Zr	0	0	0.1475(1)	0.91(4)	0.90
Sc	0	0	0.1475(1)	0.91(4)	0.10
P	0.2900(3)	0	0.25	1.07(6)	0.57
Si	0.2900(3)	0	0.25	1.07(6)	0.43
O(1)	0.1829(6)	−0.0305(4)	0.1914(4)	1.48(9)	0.71(3)
O(1′)	0.163(1)	−0.021(2)	0.207(1)	1.7(2)	0.29(3)
O(2)	0.1946(2)	0.1707(2)	0.0906(1)	1.28(5)	1.0
Na(1)	0	0	0	15.38	0.63(3)
Na(2)	−0.357(1)	0	0.25	1.07	0.30(1)
Na(2′)	−0.347(3)	0.043(3)	0.286(1)	5.51	0.16(1)

	β_{11}[a]	β_{22}	β_{33}	β_{12}	β_{13}	β_{23}
Na(1)	0.074(6)	0.074(6)	0.0050(9)	0.037(3)	0	0
Na(2)	0.002(2)	0.0004(21)	0.0012(4)	0.0002(10)	0.0003(3)	0.0006(5)
Na(2′)	0.021(5)	0.014(5)	0.0040(8)	0.010(4)	−0.0008(14)	0.002(1)

[a] The form of the anisotropic temperature factor is $\exp-(h^2\beta_{11}+k^2\beta_{22}+l^2\beta_{33}+2hk\beta_{12}+2hl\beta_{13}+2kl\beta_{23})$.

minishes. This change in position is reflected most clearly in the tetrahedral P(Si) coordination geometry. At room temperature, the P(Si)–O(1′) distance, 1.44(2) Å, is significantly shorter than the other P(Si)–O bonds while by 400°C, it is within one standard deviation of the others. This equalization of the P(Si)–O distances is accompanied, however, by an increasing distortion of the tetrahedral angles, as shown for O(2)–P(Si)–O(1′) in table 7.

The effects on the Na coordination environments are less dramatic. Though the Na(2)–O(1′) distance decreases substantially, from 2.79(2) Å at 26°C to 2.58(3) Å at 400°C, it is still 0.15 Å longer than the shortest Na(2)–O distance at 400°C. The Na(2′)–O(1′) bond distances show no temperature correlations and fall within 3 esd's of the average Na(2′)–O distance for all the refinements. The refined population of atom O(1′) (tables 2–6) decreases steadily from 26°C through 300°C and then appears to level off. Given the low occupancy of this site, the variation in thermal parameters, and the

Table 3
Positional, thermal and population parameters for 100°C refinement.

Atom	x	y	x	Biso/Beq	Pop.
Zr	0	0	0.1478(1)	0.98(4)	0.90
Sc	0	0	0.1478(1)	0.98(4)	0.10
P	0.2898(2)	0	0.25	1.03(5)	0.57
Si	0.2898(2)	0	0.25	1.03(5)	0.43
O(1)	0.1814(6)	−0.0296(3)	0.1925(3)	1.73(7)	0.78(2)
O(1′)	0.153(2)	−0.028(2)	0.208(1)	1.5(2)	0.22(2)
O(2)	0.1952(2)	0.1713(2)	0.0910(1)	1.56(4)	1.0
Na(1)	0	0	0	19.74	0.69(3)
Na(2)	−0.355(1)	0	0.25	2.45	0.33(1)
Na(2′)	−0.357(3)	0.048(3)	0.291(1)	7.85	0.15(1)

	β_{11}	β_{22}	β_{33}	β_{12}	β_{13}	β_{23}
Na(1)	0.117(8)	0.117(8)	0.0013(4)	0.058(4)	0	0
Na(2)	0.005(2)	0.003(2)	0.0026(5)	0.001(1)	0.0007(3)	0.0015(6)
Na(2′)	0.020(5)	0.013(5)	0.007(1)	0.006(4)	−0.001(1)	0.008(2)

Table 4
Positional, thermal and population parameters for 200°C refinement.

Atom	x	y	z	Biso/Beq	Pop.
Zr	0	0	0.1477(1)	1.10(4)	0.90
Sc	0	0	0.1477(1)	1.10(4)	0.10
P	0.2892(2)	0	0.25	0.98(5)	0.57
Si	0.2892(2)	0	0.25	0.98(5)	0.43
O(1)	0.1801(6)	−0.0302(3)	0.1931(2)	1.99(7)	0.82(2)
O(1′)	0.145(2)	−0.033(2)	0.209(1)	1.3(3)	0.18(2)
O(2)	0.1956(2)	0.1721(2)	0.0916(1)	1.68(4)	1.0
Na(1)	0	0	0	17.93	0.64(3)
Na(2)	−0.352(1)	0	0.25	1.96	32(1)
Na(2′)	−0.365(3)	0.051(3)	0.291(1)	8.47	0.15(1)

	β_{11}	β_{22}	β_{33}	β_{12}	β_{13}	β_{23}
Na(1)	0.092(6)	0.092(6)	0.0044(7)	0.046(3)	0	0
Na(2)	0.002(2)	0.002(2)	0.0007(10)	0.0009(3)	0.0017(7)	
Na(2′)	0.024(5)	0.021(6)	0.008(4)	0.0062(13)	0.008(2)	

general limitations of the Rietveld technique, it is difficult to assess the importance of this trend. Nevertheless, it is notable that the occupancy of the O(1′) site reaches an apparent minimum at a value that is equal, within experimental error, to the occupancy of the Na(2′) site. This limit may be a manifestation of the strong preference for Na(2′)–O(1′) interactions over the highly unfavorable 2.1 Å Na(2′)–O(1) interaction discussed earlier.

3.2. Conductivity data

Results of conductivity measurements on pressed disks of $Na_{2.5}Zr_{1.8}Sc_{0.2}Si_{1.3}P_{1.7}O_{12}$ are shown in fig. 4. The upper curve represents data reported earlier [17] which were obtained on a sample prepared at 1150°C and sintered at the same temperature. That sample contained no free ZrO_2 detectable by X-ray diffraction. The Arrhenius plot yields an excellent straight line whose slope corresponds to an activation energy of 0.30 eV, with $\sigma_{300}=4.5\times10^{-2}\ \Omega^{-1}$

Table 5
Positional, thermal and population parameters for 300°C refinement.

Atom	x	y	z	Biso/Beq	Pop.
Zr	0	0	0.1478(1)	1.20(4)	0.90
Sc	0	0	0.1478(1)	1.20(4)	0.10
P	0.2886(2)	0	0.25	1.05(5)	0.57
Si	0.2886(2)	0	0.25	1.05(5)	0.43
O(1)	0.1798(5)	−0.0303(3)	0.1938(2)	2.13(6)	0.87(2)
O(1′)	0.136(2)	−0.039(2)	0.210(1)	0.7(4)	0.13(2)
O(2)	0.1955(2)	0.1718(2)	0.0919(1)	1.92(4)	1.0
Na(1)	0	0	0	20.86	0.66(3)
Na(2)	−0.350(1)	0	0.25	1.50	0.28(1)
Na(2′)	−0.357(3)	0.043(3)	0.287(1)	7.07	0.17(1)

	β_{11}	β_{22}	β_{33}	β_{12}	β_{13}	β_{23}
Na(1)	0.103(2)	0.103(2)	0.0060(9)	0.052(4)	0	0
Na(2)	0.002(1)	0.001(2)	0.0017(4)	0.0006(11)	0.0005(3)	0.0010(7)
Na(2′)	0.025(4)	0.019(4)	0.0046(7)	0.009(4)	0.0003(12)	0.004(2)

Table 6
Positional, thermal and population parameters for 400°C refinement.

Atom	x	y	z	Biso/Beq	Pop.
Zr	0	0	0.1478(1)	1.36(4)	0.90
Sc	0	0	0.1478(1)	1.36(4)	0.10
P	0.2885(2)	0	0.25	1.17(5)	0.57
Si	0.2885(2)	0	0.25	1.17(5)	0.43
O(1)	0.1801(6)	−0.0305(3)	0.1941(2)	2.39(7)	0.86(2)
O(1′)	0.136(3)	−0.040(3)	0.209(1)	1.2(4)	0.14(2)
O(2)	0.1956(2)	0.1718(2)	0.0921(1)	2.20(4)	1.0
Na(1)	0	0	0	25.18	0.71(4)
Na(2)	−0.348(1)	0	0.25	1.83	0.28(1)
Na(2′)	−0.364(3)	0.046(3)	0.289(1)	7.10	0.17(1)

	β_{11}	β_{22}	β_{33}	β_{12}	β_{13}	β_{23}
Na(1)	0.130(9)	0.130(9)	0.0059(8)	0.065(4)	0	0
Na(2)	0.003(1)	0.0008(21)	0.0020(4)	0.0004(10)	0.0006(3)	0.0012(6)
Na(2′)	0.022(4)	0.017(4)	0.0048(7)	0.005(4)	0.0002(11)	0.005(1)

cm^{-1}. The lower curve represents data obtained on the same sample used in the present neutron diffraction study. This sample was prepared at 1050°C and sintered at the same temperature so as to minimize any structural changes caused by sintering. While the Arrhenius plot is almost parallel to that represented by the first curve, the conductivity values are a little more than half those of the sample prepared at 1150°C ($\sigma_{300}=2.7\times10^{-2}\ \Omega^{-1}\ cm^{-1}$).

Table 7
Important interatomic distances (Å) and angles (deg).

Temperature (°C)	26	100	200	300	400
Zr–O(ave.)	2.080(7)	2.072(9)	2.067(9)	2.064(10)	2.060(12)
Zr–O(range)	2.056–2.102	2.052–2.107	2.042–2.104	2.029–2.101	2.012–2.100
P/Si–O(1)	1.592(7)	1.581(6)	1.574(5)	1.561(4)	1.556(5)
P/Si–O(1′)	1.44(2)	1.47(2)	1.50(2)	1.54(2)	1.56(2)
P/Si–O(2)	1.565(2)	1.561(2)	1.561(2)	1.567(2)	1.568(2)
O(2)–P/Si–O(1′)	116.1(7)	118.7(7)	120.6(8)	122.7(9)	122.1(9)
O(1)–O(1′)	0.43(2)	0.45(2)	0.48(2)	0.53(2)	0.50(2)
Na(1)–Na(2)	3.465(4)	3.475(4)	3.486(4)	3.498(4)	3.505(4)
Na(1)–Na(2′)	2.77(3)	2.64(3)	2.59(3)	2.73(3)	2.66(2)
Na(2)–Na(2′)	0.90(3)	1.05(3)	1.09(3)	0.94(3)	1.02(2)
Na(2)–Na(2′)	4.02(3)	3.92(3)	3.87(3)	4.01(3)	4.11(2)
Na(2)–Na(2)	4.785(3)	4.797(3)	4.811(3)	4.824(3)	4.833(3)
Na(2′)–Na(2′)	3.34(4)	3.12(5)	3.08(5)	3.30(4)	3.21(4)
Na(1)–O(2)	2.650(1)	2.663(1)	2.681(1)	2.689(1)	2.696(1)
Na(2)–O(ave.)	2.68(5)	2.67(6)	2.67(5)	2.66(5)	2.66(5)
Na(2)–O(range)	2.439–2.877	2.438–2.858	2.440–2.833	2.435–2.807	2.435–2.813
Na(2′)–O(ave.)	2.54(8)	2.55(9)	2.56(9)	2.56(8)	2.56(7)
Na(2′)–O(range)	2.135–2.857	2.078–2.946	2.099–2.986	2.179–2.875	2.150–2.923
Na(2′)–O(ave.)[a]	2.60(6)	2.61(7)	2.63(7)	2.61(6)	2.62(6)
Na(2′)–O(range)[a]	2.344–2.857	2.394–2.946	2.406–2.986	2.386–2.875	2.406–2.923

[a] Omitting the short Na(2′)–O(1) distance.

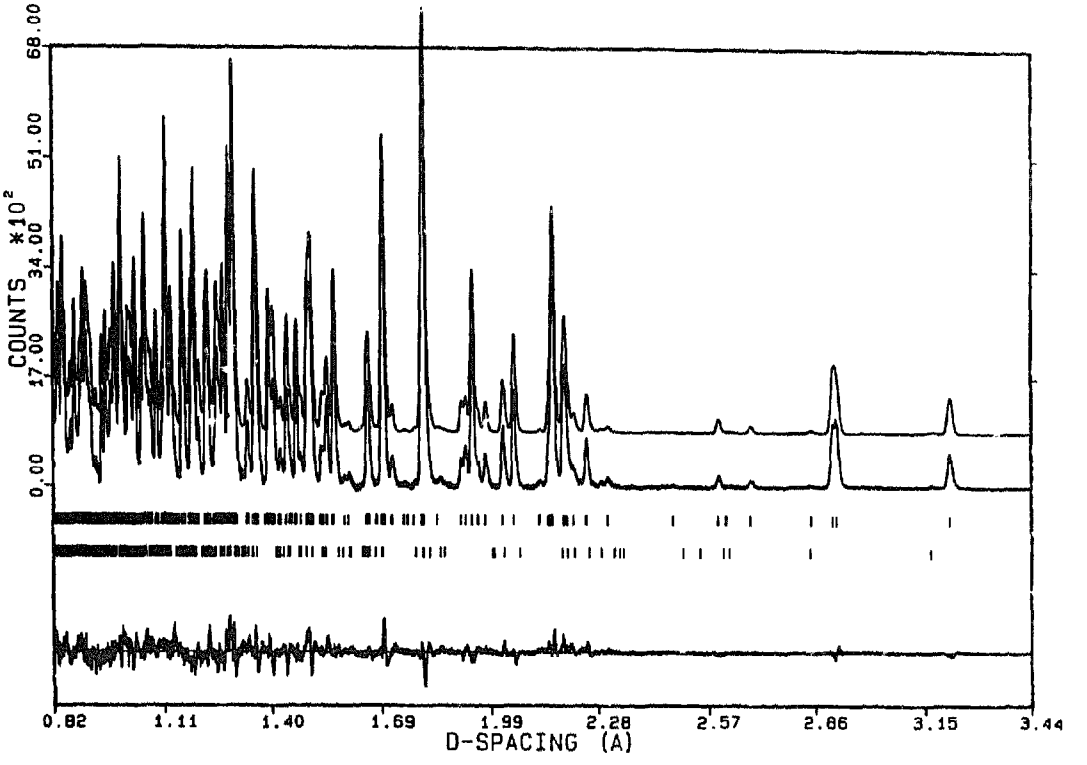

Fig. 1. Background modeled neutron TOF powder pattern at 26°C (lower) compared with calculated Rietveld refinement results (upper). The bottom trace is the difference plot and the solid vertical dashes indicate the position of Bragg reflections for $Na_{2.5}Zr_{1.8}Sc_{0.2}Si_{1.3}P_{1.7}O_{12}$ (top) and ZrO_2 (bottom).

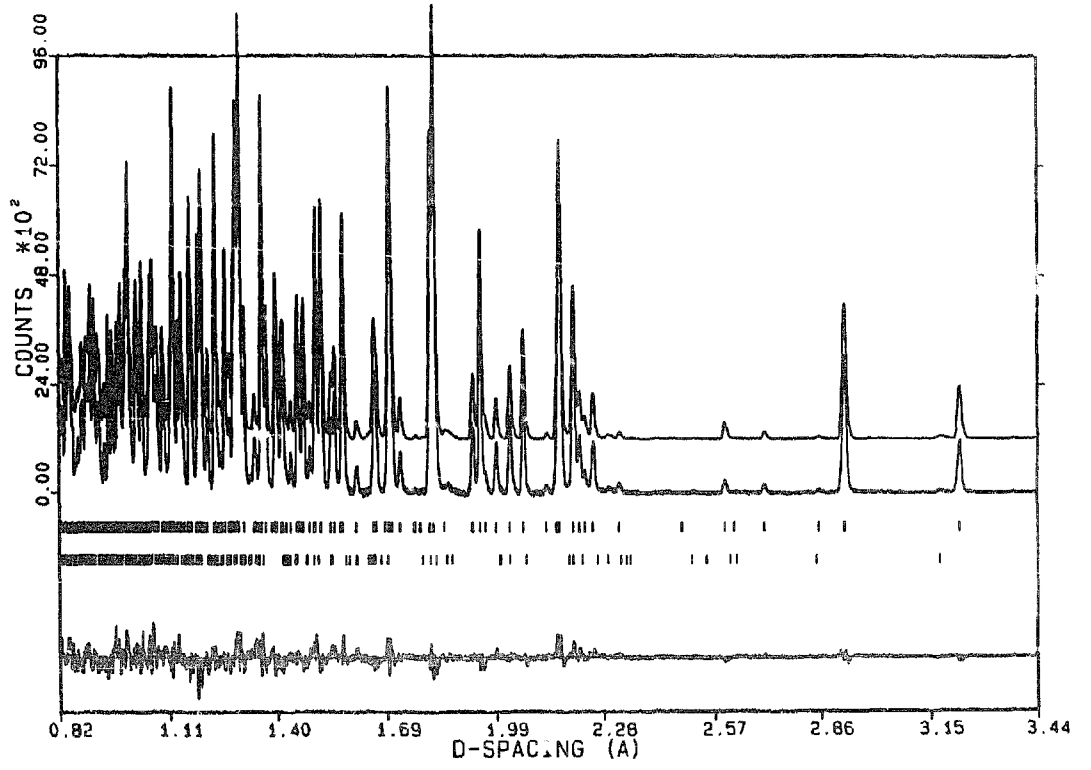

Fig. 2. Same as fig. 1 for 400°C data.

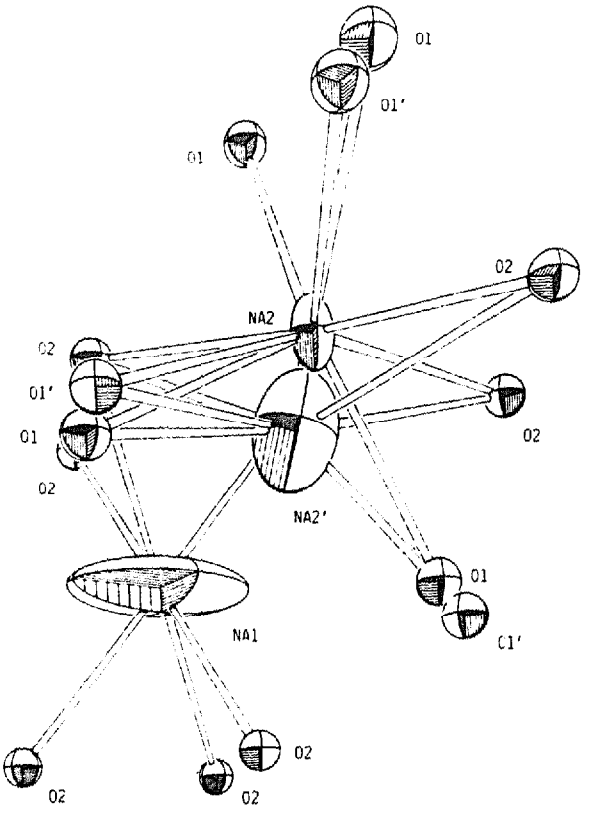

Fig. 3. Oxygen coordination and 50% thermal ellipsoids for Na(1), Na(2), and Na(2') showing the nature of the disorder.

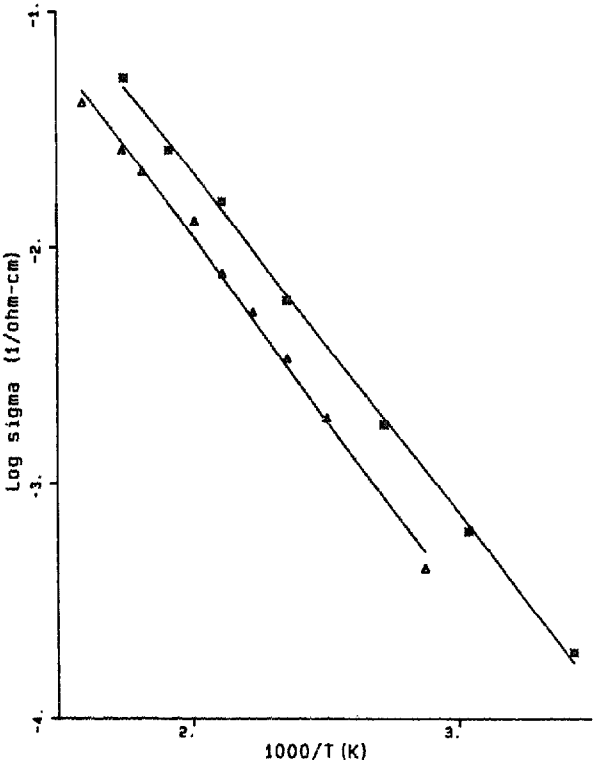

Fig. 4. Arrhenius plot of $\log(\sigma)$ versus $1/T$ for $Na_{2.5}Zr_{1.8}Sc_{0.2}Si_{1.3}P_{1.7}O_{12}$. Upper curve, sample prepared and sintered at 1150°C; lower curve, sample prepared and sintered at 1050°C (present study).

3.3. Expansion coefficients

Plots of the unit cell parameters are shown in fig. 5. From the slopes of the lines, we deduce that the linear thermal expansion coefficients are $l_a = 1.3 \times 10^{-6}$ °C^{-1} and $l_c = 2.2 \times 10^{-5}$ °C^{-1}. The corresponding volume coefficient is $\alpha_V = 2.5 \times 10^{-5}$ °C^{-1}. It should be noted that α_V decreases slightly with temperature and the value given represents an average over the temperature range 26–400°C. These average values agree well with similar values for other compositions of the rhombohedral phase [16].

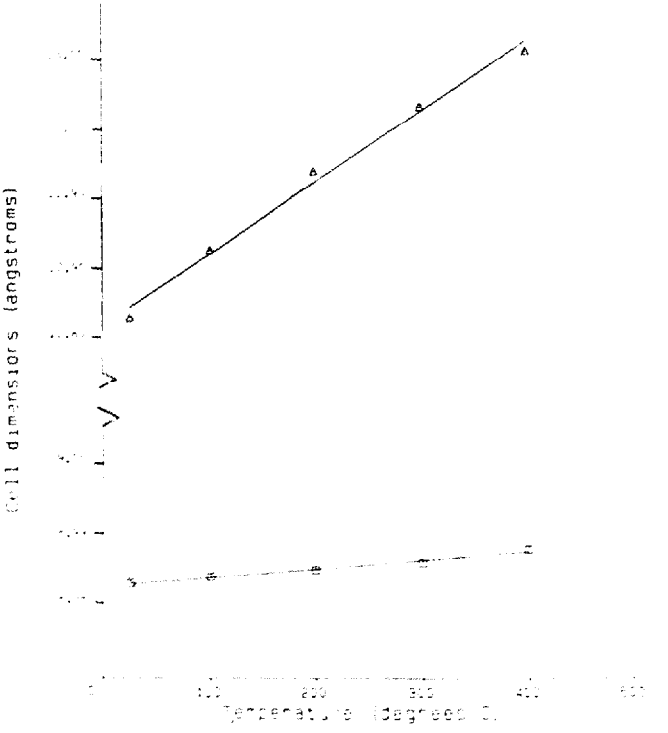

Fig. 5. Variation of the unit cell parameters of $Na_{2.5}Zr_{1.8}Sc_{0.2}Si_{1.3}P_{1.7}O_{12}$ from 26°C to 400°C.

4. Discussion

The observation in this study of split positions for Na(2) and O(1) in a rhombohedral NASICON may be compared to other recent findings of defect NASICON structures. Kohler and Schulz [11,18] have reported an interstitial Na site correlated with split

oxygen positions for the composition $Na_{3.2}Zr_{1.8}Si_{1.4}P_{1.6}O_{12}$. In this compound, however, the sodium interstitial is disordered with the zirconium rather than with the conductive sodium ions. This substitution of sodium for Zr has been observed by us in an earlier study [5] and by others [25,26] in the phase $Na_5Zr(PO_4)_3$, but never for Sc-substituted materials [17]. Indeed, we believe that in substituting for Zr^{4+}, the Sc^{3+} precludes Na^+ from occupying these sites. Hence we would not expect to see this type of static disorder in the Sc-containing compounds.

More recently, Boilot et al. [15,16] found in a variable-temperature single crystal study of the stoichiometric NASICON, $Na_3Zr_2Si_2PO_{12}$, an extra sodium position located in the conduction channel between Na(1) and Na(2) of the high temperature (350°C) rhombohedral structure. This Na disorder is present also in the low temperature (ca. 25°C) monoclinic phase but in neither case is evidence of any splitting of oxygen positions found [15]. This result is very interesting since it places the interstitial Na^+ in the same channel as we find the Na(2′) position in the present structure. These observations support the conclusion of Kohler and Schulz [11,18] that an important conduction pathway in NASICON is between Na(1) and Na(2). In addition, the interstitial Na^+ population found by Boilot et al., 11%, compares favorably with the 17% we obtained in the 400°C Rietveld refinement. However, the "mid-Na" position of Boilot et al., [15,16], is halfway between Na(1) and Na(2), ≃1.8 Å from Na(2), whereas our Na(2′) position is only ca. 1 Å from Na(2). Moreover, the occupancies of the Na(1) and Na(2) sites reported for $Na_3Zr_2Si_2PO_{12}$ (40% and 68%) are essentially opposite to what we find (cf. table 6) for $Na_{2.5}Zr_{1.8}Sc_{0.2}Si_{1.3}P_{1.7}O_{12}$. Thus our results are similar to those of Boilot et al., but with important differences which we believe may be attributed to the different synthetic techniques used in the two studies. Whereas they grew crystals "by long thermal annealing (several months) of sol/gel ceramics below the melting temperature" [15,16], we prepared our microcrystalline powder by heating a mixture of powdered oxides at ca. 1050°C over a few days. It is quite possible, therefore, that the $Na_3Zr_2Si_2PO_{12}$ structure of Boilot et al., represents a true equilibrium phase reached after a long period of heating, while our material, prepared over a much shorter period, is a non-equilibrium phase. As a result, we may have captured in progress a redistribution of the sodium ions, involving a splitting apart of the Na(2) site, which is more completely realized in $Na_3Zr_2Si_2PO_{12}$. This explanation would also account for the absence of the split oxygen, O(1′), in the equilibrium phase. In order to accommodate the interstitial Na(2′) at a bottleneck in the channel of our compound, atom O(1) is forced to move away, creating the interstitial O(1′). By contrast in $Na_3Zr_2Si_2PO_{12}$ the sodium atom has moved to the midpoint of the channel, relieving the unfavorable steric interaction with O(1). This causes the split oxygen positions to coalesce.

The distribution of sodium ions in $Na_{2.5}Zr_{1.8}Sc_{0.2}Si_{1.3}P_{1.7}O_{12}$ (tables 2–6) is in keeping with that found in the phases $Na_{3.2}Zr_{1.8}Si_{1.4}P_{1.6}O_{12}$ [10,11], $Na_3Zr_2Si_2PO_{12}$ [15,16], $Na_2Zr_2SiP_2O_{12}$ [12] and $Na_3ZrScSiP_2O_{12}$ [17] in demonstrating a consistent pattern of underoccupancy of the Na(1) site for rhombohedral NASICON phases with $x > 1$. These results contrast with earlier findings of fully occupied Na(1) sites in rhombohedral NASICONs with $x = 1.0$, 2.5, and 3.0 [3,4]. This underoccupancy is even more pronounced in the monoclinic phase [5,7,12,15]. As pointed out earlier [5–7] the underoccupancy must reflect Na^+–Na^+ repulsions since in some cases [7] the Na(1)–Na(3) distance is very short and much of the Na(3) is in an interstitial position. The repulsion is relieved by the underoccupancy, but the situation is more complex and will be described in a forthcoming paper.

What is increasingly emergent from the many NASICON studies is a picture of a complex and dynamic assemblage capable of undergoing many subtle structural rearrangements in the drive to equilibrium. The exact structure obtained appears to be highly dependent not only on composition but also on the method of preparation [14]. As a result, we believe that past structural discrepancies may be due to differences in sample preparation and that future studies on NASICON must take due cognizance of the importance of sample history on structure and conductivity.

Acknowledgement

The Intense Pulsed Neutron Source (IPNS) of Argonne National Laboratory is operated under the auspices of the U.S. Department of Energy, BES-Materials Science, under contract W-31-109-Eng-38, to whom we extend thanks for the use of their facilities. The portion of the work done at Texas A&M University was supported by a grant from the Texas A&M University Center for Energy and Mineral Resources and by the Regents of The Texas A&M University System (AUF Grant No. 24423MS, Materials and Surface Science). We thank Dr. M.A. Subramanian of E.I. du Pont de Nemours for technical assistance with the conductivity data.

References

[1] J.B. Goodenough, H.Y.-P. Hong and J.A. Kafalas, Mater. Res. Bull 11 (1976) 204.
[2] H.Y.-P. Hong, Mater. Res. Bull. 11 (1976) 173.
[3] B.J. Wuensch, L.J. Schioler and E. Prince, in: Proc. Conf. High Temperature Solid Oxide Electrolytes, Aug. 16–17, 1983, Vol. II (Brookhaven National Laboratory) p. 59.
[4] L.J. Schioler, Ph.D. dissertation (MIT, Cambridge, MA 1983).
[5] P.R. Rudolf, M.A. Subramanian, A. Clearfield and J.D. Jorgensen, Mater. Res. Bull. 20 (1985) 643; 21 (1986) 1137.
[6] A. Clearfield, M.A. Subramanian, P.R. Rudolf and A. Moini, Solid State Ionics 18/19 (1986) 13.
[7] P.R. Rudolf, A. Clearfield and J.D. Jorgensen, Solid State Ionics 21 (1986) 213.
[8] A. Clearfield, M.A. Subramanian, W. Wang and P. Jerus, Solid State Ionics 9/10 (1983) 895.
[9] H. Kohler and H. Schulz, Solid State Ionics 9/10 (1983) 795.
[10] H. Kohler, H. Schulz and O. Melnikov, Mater. Res. Bull. 18 (1983) 589.
[11] H. Kohler and H. Schulz, Mater. Res. Bull. 20 (1985) 1461.
[12] W.H. Baur, J.R. Dygas, D.H. Whitmore and J. Faber, Solid State Ionics 18/19 (1986) 935.
[13] Ph. Colomban, Solid State Ionics 21 (1986) 97.
[14] A. Moini and A. Clearfield, Adv. Ceramic Mater. 2 (1987) 173.
[15] J.P. Boilot, G. Collin and Ph. Colomban, Mater. Res. Bull. 22 (1987) 669.
[16] J.P. Boilot, G. Collin and Ph. Colomban, J. Solid State Chem. 73 (1988) 160.
[17] M.A. Subramanian, P.R. Rudolf and A. Clearfield, J. Solid State Chem. 60 (1985) 172.
[18] H. Kohler and H. Schulz, Mater. Res. Bull. 21 (1986) 23.
[19] A. Clearfield and S.P. Pack, J. Inorg. Nucl. Chem. 13 (1974) 2880.
[20] J.D. Jorgensen and J. Faber, Jr., in: Proc. 6th Meeting Int. Collab. Advan. Neutron Sources, June 28–July 2, 1982, ed. J.M. Carpenter (Argonne National Laboratory) pp. 105–114 (ANL Publ. ANL-82-80).
[21] J.D. Jorgensen and F. Rotella, J. Appl. Crystallogr. 15 (1982) 27.
[22] J.D. McCullough and K.N. Trueblood, Acta Crystallogr. 12 (1959) 507.
[23] R.B. Von Dreele, J.D. Jorgensen and C.G. Windsor, J. Appl. Crystallogr. 15 (1982) 581.
[24] C.T. Prewitt and R.D. Shannon, Trans Am. Crystallogr. Assoc. 5 (1969) 57.
[25] J.P. Boilot, G. Collin and R. Comes, J. Solid State Chem. 50 (1983) 91.
[26] S.J. Milne, J.A. Gard and A.R. West, Mater. Res. Bull. 20 (1985) 557.